

10-6-2009

Josephson scanning tunneling microscopy: A local and direct probe of the superconducting order parameter

Richard P. Barber Jr.
Santa Clara University, rbarber@scu.edu

Hikari Kimura

Shuhei Ono

Yoichi Ando

Robert C. Dynes

Follow this and additional works at: <http://scholarcommons.scu.edu/physics>

Recommended Citation

Hikari Kimura, R. P. Barber, Jr., S. Ono, Yoichi Ando and R. C. Dynes, "Josephson scanning tunneling microscopy - a local and direct probe of the superconducting order parameter," *Physical Review B*, 80, 144506, (2009).

Josephson scanning tunneling microscopy: A local and direct probe of the superconducting order parameter

Hikari Kimura,^{1,2,*} R. P. Barber, Jr.,³ S. Ono,⁴ Yoichi Ando,⁵ and R. C. Dynes^{1,2,6,†}

¹*Department of Physics, University of California, Berkeley, California 94720, USA*

²*Materials Sciences Division, Lawrence Berkeley National Laboratory, Berkeley, California 94720, USA*

³*Department of Physics, Santa Clara University, Santa Clara, California 95053, USA*

⁴*Central Research Institute of Electric Power Industry, Komae, Tokyo 201-8511, Japan*

⁵*Institute of Scientific and Industrial Research, Osaka University, Ibaraki, Osaka 567-0047, Japan*

⁶*Department of Physics, University of California–San Diego, La Jolla, California 92093-0319, USA*

(Received 10 August 2009; revised manuscript received 15 September 2009; published 6 October 2009)

Direct measurements of the superconducting superfluid on the surface of vacuum-cleaved $\text{Bi}_2\text{Sr}_2\text{CaCu}_2\text{O}_{8+\delta}$ (BSCCO) samples are reported. These measurements are accomplished via Josephson tunneling into the sample using a scanning tunneling microscope (STM) equipped with a superconducting tip. The spatial resolution of the STM of lateral distances less than the superconducting coherence length allows it to reveal local inhomogeneities in the pair wave function of the BSCCO. Instrument performance is demonstrated first with Josephson measurements of Pb films followed by the layered superconductor NbSe_2 . The relevant measurement parameter, the Josephson $I_C R_N$ product, is discussed within the context of both BCS superconductors and the high transition temperature superconductors. The local relationship between the $I_C R_N$ product and the quasiparticle density of states (DOS) gap are presented within the context of phase diagrams for BSCCO. Excessive current densities can be produced with these measurements and have been found to alter the local DOS in the BSCCO. Systematic studies of this effect were performed to determine the practical measurement limits for these experiments. Alternative methods for preparation of the BSCCO surface are also discussed.

DOI: [10.1103/PhysRevB.80.144506](https://doi.org/10.1103/PhysRevB.80.144506)

PACS number(s): 74.40.+k, 74.25.Dw, 74.50.+r, 74.72.Hs

I. INTRODUCTION

Scanning tunneling microscopy (STM) and scanning tunneling spectroscopy (STS) have been extensively utilized for nanometer scale studies of physical and electronic structures on the surface of high transition temperature (high- T_C) superconducting cuprates, especially $\text{Bi}_2\text{Sr}_2\text{CaCu}_2\text{O}_{8+\delta}$ (BSCCO) and $\text{YBa}_2\text{Cu}_3\text{O}_{7-\delta}$ (YBCO). A rich array of experiments includes imaging vortex flux lines^{1–3} and mapping the integrated local density of states (LDOS).^{4–6} These latter results were used to determine a gap 2Δ taken to be the difference between two coherence peaks in the LDOS. The spatial resolution combined with spectroscopic results has been used to produce “gap maps” over the surface for various dopings in BSCCO. These studies have revealed that (i) the formation of gapped regions obtained from the dI/dV spectra actually start above T_C , and there is a linear relation between Δ and the gap opening temperature, T^* (Ref. 7); and (ii) there is an anticorrelation between the energy gap Δ in the superconducting state and the normal state conductance at the Fermi energy⁸ for various dopings of BSCCO. A challenge with this approach is that the identification of Δ becomes ambiguous in strongly underdoped BSCCO where the observed dI/dV curves no longer have well-defined sharp coherence peaks.^{9,10}

Although these STM/STS experiments on high- T_C superconductors have yielded a wealth of data, they suffer from important limitations. Of particular significance in our opinion is that because they utilize a normal metal tip, these studies can only probe the local *quasiparticle* density of states (DOS). This DOS almost certainly has an intimate connection with the superconductivity in these materials;

however, that relationship is still unknown. Furthermore, the derived gap qualitatively changes its shape with doping. In contrast, the BCS theory for conventional superconductors defines a well-established relationship between the gap in the quasiparticle DOS (Δ_{BCS}) and fundamental quantities of the superconducting state including the amplitude of the order parameter and the superconducting transition temperature, T_C . Without a similar theory for the high- T_C superconductors to enable the inference of the superconducting properties from the quasiparticle DOS, it is necessary to directly probe the superconducting superfluid of these materials. Two central questions that such a direct probe should address are (i) whether the superconducting order parameter of BSCCO has spatial variation and (ii) how the superconducting ground state correlates with the quasiparticle excited states (Δ).

In this paper we will present the results of experiments using an STM with a superconducting tip. This instrument allows us to directly probe the superconducting superfluid at the surface of BSCCO using the Josephson effect. We will first discuss the primary quantity derived from Josephson tunneling measurements, the $I_C R_N$ product, and its relationship to the fundamental properties of the superconductors that make up the tunnel junction. After a description of the technical aspects of the apparatus, data which verify its successful operation on a conventional superconductor (Pb) will be presented. The approach is then extended to a layered superconductor (NbSe_2) and then finally to the high- T_C superconductor BSCCO. BSCCO is believed to be primarily a *d*-wave superconductor but with a weak *s*-wave component. Furthermore, the STM probes the order parameter at the surface where the symmetry restrictions might be relaxed somewhat. This experiment relies on coupling to the *s*-wave component.

II. $I_C R_N$ PRODUCT

Josephson tunneling is Cooper pair tunneling between two superconductors separated by a thin barrier. The zero-voltage supercurrent flowing through the junction is given by $I = I_C \sin(\varphi_2 - \varphi_1)$, where I_C is the maximum zero temperature supercurrent that the junction can sustain and $\varphi_{1(2)}$ is the phase of two superconducting electrodes' order parameter. The maximum supercurrent is related to the amplitude of the superconducting pair wave function. An STM with a superconducting tip can be a local Josephson probe and can, in principle, access the superconducting pair wave function directly on a length scale smaller than or comparable to the superconducting coherence length, ξ .

Between the two superconductors in a tunnel junction, the Josephson $I_C R_N$ product (R_N is the normal state resistance of the junction) is a directly measurable quantity uniquely determined by the specific materials. $I_C R_N$ is a fundamental parameter that is directly linked to the superconducting order parameter amplitude $|\Psi|$, and in the case of conventional superconductors to the energy gaps Δ_{BCS} through the BCS relationship.¹¹ Josephson studies using a superconducting STM on conventional superconductors have shown good agreement between the measured $I_C R_N$ and BCS predictions.^{12,13} For high- T_C superconductors, on the other hand, there is no established theory to relate $I_C R_N$ with Δ derived from the quasiparticle excitation spectrum. There can be at least two additional issues not present for conventional superconductors. The first is that we do not have a universally agreed-upon theory of the high- T_C cuprates and second, the symmetry of the order parameter has a substantial $d_{x^2-y^2}$ component thus making the coupling to a conventional superconductor (s -wave symmetry) more complicated. An $I_C R_N$ measurement on BSCCO using a conventional superconducting STM should, however, both prove the existence and yield the amplitude of the BSCCO pair wave function that couples to the conventional superconducting tip. Because of the spatial resolution of an STM, this measurement could reveal useful information regarding inhomogeneities in the superconductivity of BSCCO.

III. EXPERIMENT

A. Superconducting tip

A reproducible and stable superconducting tip fabrication method that we have developed begins with a $\text{Pt}_{0.8}/\text{Ir}_{0.2}$ tip mechanically cut from a 0.25 mm diameter wire.¹⁴ Tips are then placed in a bell-jar evaporator with the tip apex pointing toward the evaporation sources. 5500 Å of Pb is deposited at a rate of ~ 40 Å/s followed by 36 Å of Ag at a rate of 1 Å/s without breaking vacuum. The thick layer of Pb was chosen such that at 2.1 K, well below transition temperature of Pb ($T_C = 7.2$ K), there would be bulk superconductivity in the tip (superconducting coherence length, ξ_0 , of Pb is $\xi_0 = 830$ Å). The Ag serves as a capping layer to protect the Pb layer from rapid oxidation upon exposure to the atmosphere. The Ag layer is thin enough to proximity couple to the Pb layer resulting in a superconducting tip with T_C and Δ_{BCS} only slightly below that of bulk Pb. Because the Pb/Ag bi-

layer is deposited without breaking vacuum, the interface between the layers is expected to be clean, and thus superconductivity may be induced in the Ag layer by the proximity effect.¹⁵ The Pb/Ag combination is also a good metallurgical choice, as there is no significant alloying at the interface.¹⁶ For Josephson measurements of a conventional superconductor, Pb/Ag samples were also evaporated onto freshly cleaved graphite substrates during the same deposition as the tips. The same Ag capping layer keeps these samples stable for the transfer from the evaporator to the STM apparatus.

B. NbSe_2

Single-crystal $2H\text{-NbSe}_2$ was chosen as a first target material beyond conventional superconductors as a surrogate to the high- T_C superconducting cuprates. $2H\text{-NbSe}_2$, a family of layered transition-metal dichalcogenides, is a type-II conventional superconductor with $T_C = 7.2$ K and charge-density wave (CDW) transition at $T_{\text{CDW}} = 33$ K, so the CDW state coexists with the superconducting state below T_C . This material also has short coherence lengths ($\xi_{a,b} = 77$ Å and $\xi_c = 23$ Å), an anisotropic s -wave gap varying from 0.7 to 1.4 meV across the Fermi surface¹⁷ and multiband superconductivity indicated from observations of momentum-dependent superconducting gap on the different Fermi surface sheets.¹⁸ Van der Waals bonding between Se layers is so weak that the crystal is easily cleaved to expose a fresh and inert surface for STM measurements. However, no Josephson tunneling measurements have been reported before those of our group¹³ partly because it is difficult to grow a stable insulating (usually oxide) layer for planar tunnel junctions.

C. $\text{Bi}_2\text{Sr}_2\text{CaCu}_2\text{O}_{8+\delta}$

There is still much discussion and controversy about the symmetry of the order parameter of high- T_C superconducting cuprates and whether the pseudogap state observed in the underdoped region in BSCCO is a precursor to the coherent superconducting state. If the symmetry is strictly d -wave, there should exist no Josephson coupling between high- T_C superconducting cuprates and a conventional superconducting tip. However, Josephson coupling has been observed between conventional superconductors and YBCO (Ref. 19) as well as BSCCO.^{20,21} Thus, Josephson measurements of BSCCO using a superconducting STM should reveal results about the symmetry of the BSCCO order parameter. Correlations between $I_C R_N$ products from the Josephson effect and the energy gap Δ measured from the quasiparticle excitation spectra of BSCCO should contribute to the construction of a microscopic theory of the mechanism of high- T_C superconducting cuprates. An apparent constraint indicated by a previous study of BSCCO at high STM currents⁵ that we will discuss later is that there is a threshold current above which the BSCCO morphology and spectroscopy are drastically and irreversibly changed. This effect appears at a tunneling current of about 500 pA. Care will be taken to sweep the bias of the STM junction such that the resulting tunneling current does not exceed this threshold to avoid changing the BSCCO electronic structure.

BSCCO single crystals are grown by the floating zone method²² with the hole doping, δ_h , ranging between heavily underdoped ($T_C=64$ K) and overdoped ($T_C=74$ K) via optimally doped samples ($T_C=94$ K). T_C was determined by magnetic susceptibility measurements. In these current studies, extensive Josephson measurements were performed on overdoped samples with different dopings ($T_C=76, 79$, and 81 K). Our BSCCO samples which have typical dimensions of 1 mm \times 1 mm and a few tens of μm thick are glued onto a copper plate with silver epoxy (Epoxy technology EE 129–4). All of the samples were cleaved in high vacuum ($\sim 3 \times 10^{-8}$ Torr) at room temperature to expose a fresh surface. BiO-BiO planes are attracted by weak van der Waals bonding so that they are most likely the cleavage plane,²³ with the conducting CuO_2 surface two layers below. Cleaved samples are then cooled to $T=2.1$ K after being inserted into the STM. The experiments are performed at 2.1 K where the properties of Pb approach the low temperature limit. While lower temperatures would nominally reduce the fluctuations, we find that a characteristic noise temperature T_n of the apparatus dominates the fluctuations. A lower base temperature in the current configuration would therefore not improve the measurements; only a significant reduction in the noise leakage from room-temperature electronics would do so.

D. E_J , phase fluctuations, T_n , current density

The signature Josephson response of a superconducting STM differs from that of typical low R_N planar S/I/S devices. For identical superconductors, Ambegaokar and Baratoff¹¹ derived the temperature-dependent Josephson binding energy, E_J , where

$$E_J(T) = \frac{\hbar I_C}{2e} = \frac{\pi \hbar \Delta(T)}{4e^2 R_N} \tanh\left(\frac{\Delta(T)}{2k_B T}\right). \quad (1)$$

Because of the experimental base temperature ($T=2.1$ K) and large R_N associated with an STM, E_J is smaller than $k_B T$ for the Josephson STM. For example, with an STM resistance of 50 k Ω , E_J/k_B is roughly 1 K. Also for ultrasmall tunnel junctions, the Coulomb charging energy E_C can be large. We estimate the capacitance, C , of the STM junction formed between the conical tip apex and the sample surface to be about 1 fF. $E_C=e^2/2C$ is therefore of order 1 K: comparable to both E_J and $k_B T$. The time scale of an electron tunneling in the STM junction and conducting off the tip is much shorter than \hbar/E_C , so that the electron is swept away long before the charging effects become relevant. Because $k_B T$ is the dominant energy, the phase difference of the two superconductors, φ , is not locked in a minimum of the sinusoidal E_J vs φ washboard potential but is thermally excited and diffusive (Fig. 1). With a current bias, the phase diffuses preferentially in one direction as illustrated in Fig. 1. Near zero-bias voltage the observed Josephson current is therefore dependent on the bias due to the dissipative phase motion.

The phase diffusion model was first proposed by Ivanchenko and Zil'berman²⁴ and further developed by others.^{25,26} In this model we can consider the thermal fluctuations as Johnson noise generated by a resistor Z_{ENV} at a noise temperature T_n ; both parameters depend only on the

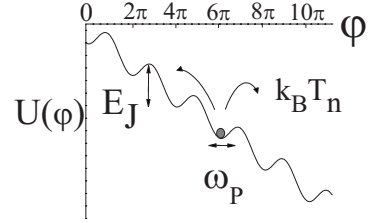


FIG. 1. Josephson phase dynamics of the washboard potential in the classical thermal fluctuation regime.

experimental setup. In the limit of $\alpha=E_J/k_B T_n \leq 1$, they derived a simple analytic form for the I - V characteristics of the thermally fluctuated Josephson currents,

$$I(V) = \frac{I_C^2 Z_{ENV}}{2} \frac{V}{V^2 + V_P^2}. \quad (2)$$

As described above, the relevant energy scale of our STM Josephson junctions is $\alpha \leq 1$, so that the analytic form of Eq. (2) is applicable to analyzing our data.

Now the pair current has a voltage dependence due to the diffusive phase motion. V_P as a function of T_n and Z_{ENV} is the voltage where the pair current becomes maximum. V_P will not change if T_n and Z_{ENV} are constant parameters intrinsic to the junction's environment, while I_C increases as R_N is decreased. Thus, the thermally fluctuated Josephson current is characterized by three quantities, maximum supercurrent I_C , T_n , and Z_{ENV} . T_n is an effective noise temperature for the ultrasmall junction. This temperature can be elevated by noise from the room-temperature electronics unless all the leads connecting to the junction are heavily filtered. Z_{ENV} is the impedance of the junction's environment or the electronic circuit where the junction is embedded. It is reported that for ultrasmall tunnel junctions, the Josephson phase dynamics is at very high frequency characterized by the Josephson plasma frequency, ω_P or E_J/\hbar (for STM Josephson junctions, it is of order of $10^{11} \sim 10^{12}$ Hz) and the frequency-dependent damping at this frequency region is dominated by stray capacitance and inductance of the cables connecting the junction to the external circuit.^{27–30} The cables will load the junction with an impedance on the order of the free space impedance, $Z_0 = \sqrt{\mu_0/\epsilon_0} = 377 \Omega$.

Experimentally we are interested in determining the Josephson $I_C R_N$ product, a quantity characteristic of the superconductivity of the constituent materials. If we observe the phase diffusion branches in our STM Josephson junctions, we can characterize them by identifying the two parameters, T_n and Z_{ENV} , and then we can directly derive $I_C R_N$ of the material of interest by comparing the observed data and fits to the phase diffusion model.

Another concern for implementing a Josephson STM is the high current density due to the small geometry of the STM junction. A low junction resistance is desired such that E_J is maximized, but it results in a high current density. In this configuration the current density, j , can be calculated using the tunnel current $I=10$ nA which is a typical value for Pb/I/Pb STM Josephson junctions and the effective diameter of the superconducting tip, $\sim 3 \text{ \AA}$ (for fcc structure of

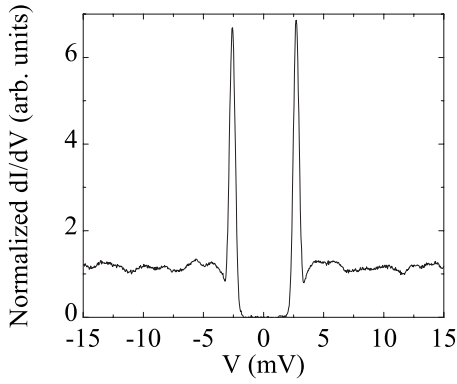


FIG. 2. Normalized dI/dV spectrum of a Pb/I/Pb STM junction at $T=2.1$ K. The Pb phonon structures can be seen as dips at 7 and 12 mV: energies corresponding respectively to the transverse and longitudinal phonon energies in Pb as measured from the energy gap edge.

Ag, the nearest-neighbor distance is 2.89 \AA) over which electrons are being injected. This calculation yields $j \sim 10^7 \text{ A/cm}^2$, a very high current density. Nevertheless, as presented later, Josephson current was observed using the SC STM tip and no self-heating effect due to the high current density was observed for Pb and NbSe₂.³¹ For BSCCO, however, previous work reported that the high current density caused a huge effect on both its electronic structure and morphology.⁵

IV. EXPERIMENTAL RESULTS

A. Pb

To test the operation of our SC-STM, we first studied Ag-capped Pb films with our Ag-capped Pb tip (a symmetric junction). The spectrum we obtained is shown in Fig. 2 and is characteristic of S/I/S tunnel junctions: very sharp coherence peaks corresponding to $eV = \pm(\Delta_{\text{tip}} + \Delta_{\text{sample}})$, from which we obtained $\Delta_{\text{tip}} = \Delta_{\text{sample}} = 1.35 \text{ meV}$, slightly smaller than the bulk value for Pb ($\Delta_{\text{bulk}} = 1.4 \text{ meV}$) due to the proximity effect of the Ag capping layer. Moreover, the deviations from the BCS density of states outside the Pb gap due to strong-coupling effects are clearly seen at energies corresponding to the transverse and longitudinal phonon energies, $eV_T - 2\Delta = 4.5 \text{ meV}$ and $eV_L - 2\Delta = 8.5 \text{ meV}$, respectively. Furthermore, just above the large coherence peaks we see the effects of the Ag proximity on the superconducting Pb. This shows up as a small dip just above the peak at 2Δ . Figure 3 presents several $I-V$ curves measured at different R_N by changing the tip-sample distance sequentially. The superconducting gap size remains unchanged as R_N is decreased. Low leakage current below the Pb gap (shown in Fig. 3) and the observation of the phonon structure in Fig. 2 confirm high quality vacuum tunnel junctions. To acquire these $I-V$ characteristics, the tunnel current feedback loop is temporarily turned off only during the measurement. We find that in the time required to do these measurements and the Josephson measurements later, the tip position remains stable. The feedback is re-established immediately after each $I-V$ acquisition.

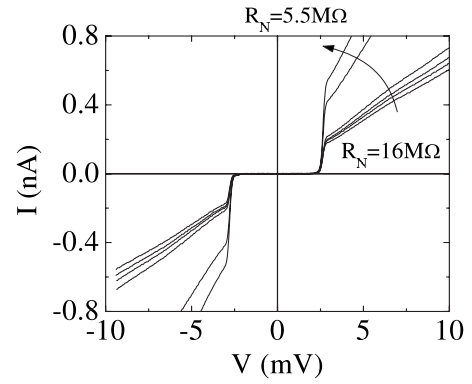


FIG. 3. $I-V$ characteristics of Pb/I/Pb STM junctions at $T=2.1$ K. $I-V$ curves are measured as the junction normal state resistance R_N is varied (z position) with the tip position (x, y) fixed. At these high resistances, E_J is too small for the Josephson effects to be observable. Also Coulomb blockade effects are negligible because the resistance of the tip and the film is such that the charge is swept away on a short time scale compared with E_C .

Figure 4 shows the observed $I-V$ characteristics at lower voltages (lines) for STM Josephson junctions formed between a Pb/Ag superconducting tip and a Pb/Ag superconducting film. The top panel of Fig. 4 shows that the location

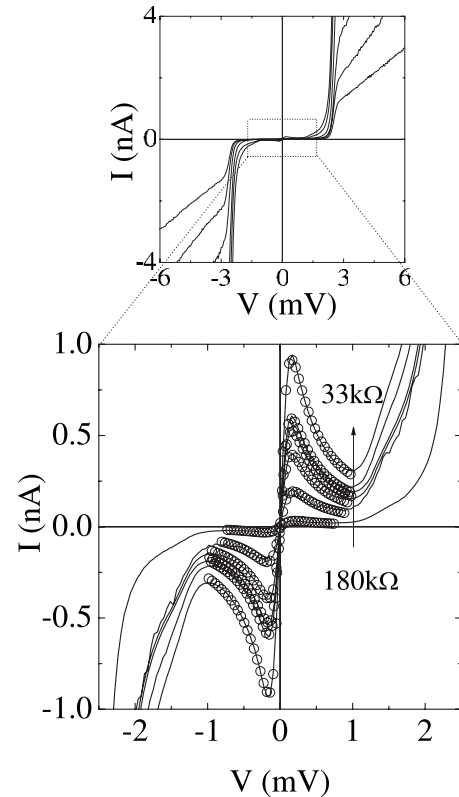


FIG. 4. $I-V$ characteristics of Pb/I/Pb STM junctions at $T=2.1$ K. (Top panel) Apparent are both the onset of the tunnel current at $V=2\Delta$ and structures near zero bias (inside the box). (Bottom) $I-V$ characteristics near zero bias for lower junction resistances than those in the top frame. The lines display the measured thermally fluctuated Josephson current and the symbols represent two-parameter fits to the phase diffusion model.

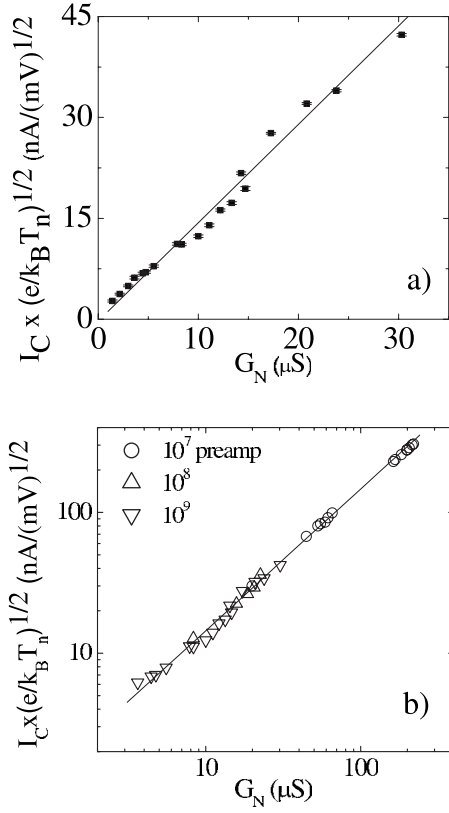


FIG. 5. (a) Plot of $I_C \times \sqrt{e/k_B T_n}$ vs G_N of Pb/I/Pb STM junctions. The slope is equal to $I_C R_N \times \sqrt{e/k_B T_n}$ and is shown as a linear fit. From the fitted slope and using the known value of $I_C R_N$ (Pb/I/Pb), T_n and Z_{ENV} are determined to be 15.9 ± 0.1 K and 279 ± 9 Ω , respectively. (b) Log-log plot of $I_C \times \sqrt{e/k_B T_n}$ vs G_N for data from three different preamplifiers [including that from (a)]. All data fall onto the same single line indicating T_n does not change due to large current flowing through the tunnel junction. These results give us confidence in using these two parameters T_n and Z_{ENV} later in our determination of $I_C R_N$ for NbSe₂ and BSCCO.

of the gap does not change as R_N is lowered. The bottom panel is a close-up view of I - V characteristics near zero bias and clearly shows peaked structures first appearing and then exhibiting increasing heights as R_N is decreased (E_J enhanced). These observed I - V curves are fitted to the phase diffusion model [Eq. (2)] with two parameters, V_P and I_C .

The best fits to the phase diffusion model are represented by the symbols in the bottom panel of Fig. 4 and the quality of these fits convince us that we have observed the signature of pair tunneling. This analysis yields a plot of $I_C \times \sqrt{e/k_B T_n}$ vs $G_N = 1/R_N$, expected to be linear with zero intercept (no I_C at infinite R_N) and a slope equal to $I_C R_N \times \sqrt{e/k_B T_n}$, as shown in Fig. 5(a). We can calculate $I_C R_N$ of Pb from the Ambegaokar-Baratoff formula¹¹ or Eq. (1) using $\Delta = 1.35$ meV at $T = 2.1$ K and including a factor of 0.788 due to strong electron-phonon coupling in Pb.³² For $T = 2.1$ K and T_C (Pb) = 7.2 K, the hyperbolic tangent is very close to unity and we get $I_C R_N$ (Pb/I/Pb) = 1.671 mV. Substituting this value into the slope of the linear data fit in Fig. 5(a) for our STM Josephson junctions, we can determine T_n and Z_{ENV} , which are parameters depending only on the experimental setup. Current values of these quantities for our

apparatus are 15.9 ± 0.1 K and 279 ± 9 Ω , respectively. The fact that T_n is higher than the 2.1 K base temperature can be explained by leakage of rf noise to the junction from room-temperature electronics. This value for T_n is an improvement from our earlier work as a result of low temperature filters inserted close to the microscope. Further improvements are called for as T_n is still higher than 2.1 K. Z_{ENV} is close to the expected value of the impedance of free space as described above. These quantities were measured using a preamplifier with 10^9 gain. We repeated the Josephson measurements to derive T_n and Z_{ENV} using other preamplifiers with lower gains (10^7 and 10^8) to cover the larger tunneling current range. All three data sets of the $I_C R_N$ plots in Fig. 5(b) fall on the same single line, convincing us that the Josephson coupling is enhanced as R_N is decreased and T_n and Z_{ENV} are constant parameters intrinsic to the experimental circumstances and configuration. This also indicates that T_n remains the same even for high current density (lower R_N). No heating effects or degraded superconducting DOS of the Pb tip or sample were observed.

The lowest junction normal state resistance we studied was 4.6 k Ω , which is smaller than the quantum resistance of a single channel in the ballistic regime, $R_Q = h/2e^2 = 12.9$ k Ω . Subharmonic gap structures observed in the Pb/I/Pb STM Josephson junctions indicate that the low resistance STM junction is not in the weak tunneling limit ($|T|^2 = D = 10^{-6}$ or smaller), but somewhat higher transparency, $D \sim 0.1$, contributed from several conduction channels.³³

B. NbSe₂

The data of Pb/I/NbSe₂ STM Josephson junctions are presented in Fig. 6. The experimental data on the bottom panel (lines) are contributions from the thermally fluctuated Josephson currents after subtraction of the quasiparticle background due to thermally excited quasiparticles. The background is obtained from the I - V curves of high resistance junctions where no Josephson currents are observed. Figure 6 shows good agreement between the fits to the phase diffusion model (symbols) and the observed data. Since the slope value in Fig. 7 is equal to $I_C R_N \times \sqrt{e/k_B T_n}$ and we can assume that T_n and Z_{ENV} remain constant, we can write a relationship $\sqrt{k_B T_n}/e = I_C R_N(\text{Pb})/\text{slope}(\text{Pb}) = I_C R_N(\text{Pb}/\text{NbSe}_2)/\text{slope}(\text{Pb}/\text{NbSe}_2)$, where $\text{slope}(\text{Pb})$ is obtained from the linear fit to the data in the $I_C \times \sqrt{e/k_B T_n}$ vs G_N plot of the Pb/I/Pb STM Josephson junctions shown in Fig. 5. Substituting the known values, $I_C R_N(\text{Pb})/\text{slope}(\text{Pb})$ and the measured $\text{slope}(\text{Pb}/\text{NbSe}_2)$, we obtain $I_C R_N(\text{Pb}/\text{NbSe}_2) = 1.39 \pm 0.03$ mV. We then use the formula for the Josephson binding energy for different superconductors at $T = 0$ K given the gaps of each³⁴

$$E_J = \frac{\hbar}{e^2 R_N} \frac{\Delta_1 \Delta_2}{\Delta_1 + \Delta_2} K\left(\frac{|\Delta_1 - \Delta_2|}{\Delta_1 + \Delta_2}\right), \quad (3)$$

where $K(x)$ is a complete elliptic integral of the first kind. Substituting $\Delta_1 = \Delta_{\text{Pb}} = 1.35$ meV and Δ_2 for the smallest and average gap of NbSe₂, that is, 0.7 and 1.1 meV, respectively, into Eq. (3) yields 1.34 mV $< I_C R_N(\text{Pb}/\text{NbSe}_2, T = 0$ K)

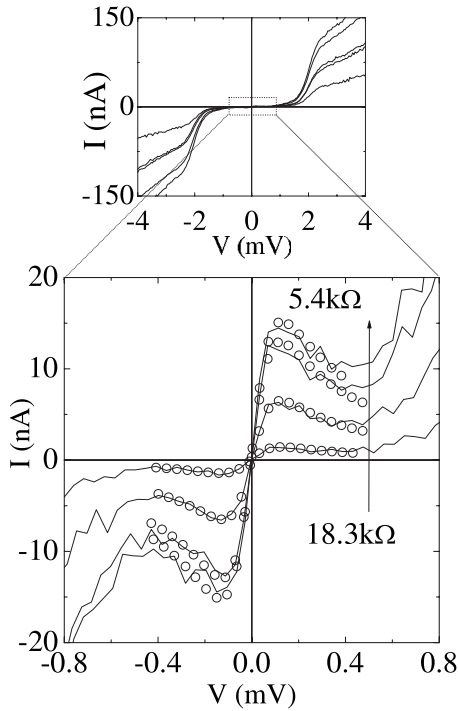


FIG. 6. *I-V* characteristics of Pb/I/NbSe₂ STM junctions at *T* = 2.1 K. (Top panel) Apparent is a current rise at $V = \Delta_{\text{Pb}} + \Delta_{\text{NbSe}_2}$. (Bottom) *I-V* characteristics near zero bias for lower junction resistances than those in the top frame showing thermally fluctuated Josephson current. The symbols represent two-parameter fits to the phase diffusion model.

< 1.70 mV. Our result of 1.39 mV is in good agreement with the theoretical expectation.

C. Bi₂Sr₂CaCu₂O_{8+δ}

Figure 8 is an atomic resolution image of cleaved optimally doped BSCCO scanned by the superconducting STM tip at *T* = 2.1 K. Because of the thick Pb layer used in our superconducting tip fabrication, it is difficult to routinely obtain atomic resolution images. However, we can easily locate

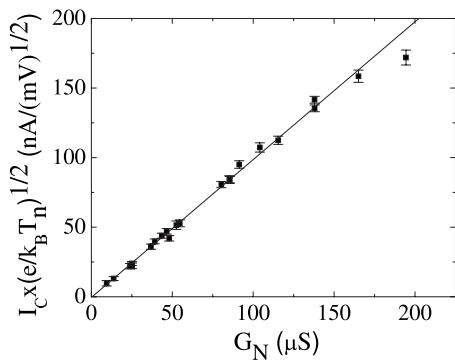


FIG. 7. Plot of $I_C \times \sqrt{e/k_B T_n}$ vs G_N for Pb/I/NbSe₂ STM junctions. The slope is equal to $I_C R_N \times \sqrt{e/k_B T_n}$ and is shown as a linear fit to the data. From the fitted slope and using the known value of $T_n = 15.9$ K, $I_C R_N$ (Pb/NbSe₂) is determined.

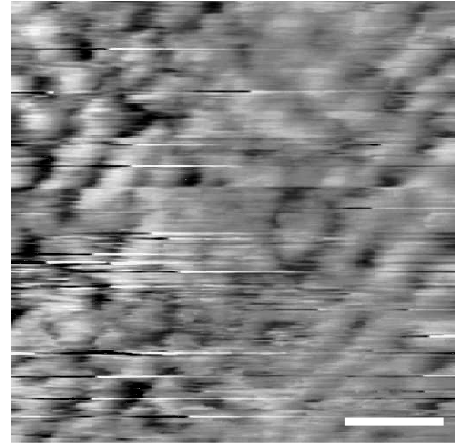


FIG. 8. Optimally doped BSCCO topography scanned by superconducting STM tip at *T* = 2.1 K. The white bar is equal to 10 Å.

step edges and isolate flat surfaces where all the present data were obtained.

S/I/S STM junctions formed between the superconducting Pb tip and overdoped BSCCO single crystals show different features than those observed for the Pb/I/Pb STM junctions. First, the energy gap of BSCCO is an order of magnitude larger than the Pb gap and second, the *dI/dV* spectrum for the BSCCO gap has a “gaplessness”—nonzero conductance at the Fermi energy—with an asymmetric normal state background conductance. Figure 9(a) presents an *I-V* characteristic of Pb/I/overdoped BSCCO STM junctions at *T* = 2.1 K taken at $R_N = 10$ MΩ clearly showing the Pb gap around 1.4 meV. The Pb gap edge does not have a sharp onset of tunnel current compared to that of Pb/I/Pb STM junctions because states exist all the way to the Fermi energy in the density of states of BSCCO. In other words, quasiparticles can tunnel at the Fermi energy of BSCCO. The inset of Fig. 9(a) shows a *dI/dV* spectrum in the region of the Pb gap. The conductance outside the Pb gap is affected by the large energy gap of BSCCO ($\Delta_{\text{BSCCO}} = 40$ meV as measured by the energy of the coherence peak.). Figure 9(b) shows a *dI/dV* spectrum taken with a large sweep range for the local density of states of BSCCO at the same location ($R_N = 500$ MΩ).

For the local Josephson measurements for BSCCO single crystals, we first observe the *dI/dV* spectrum at a particular surface point on overdoped BSCCO ($T_C = 79$ K) in order to measure the energy gap Δ (solid line in the inset of Fig. 10). We use standard lock-in techniques with 1 kHz modulation and a 2.5 mV_{RMS} modulation voltage on the bias voltage and a junction normal resistance, $R_N \sim 500$ MΩ. Although it is clearly a simplification of a more complex structure, we use the same definition for Δ as in previous works³⁵ in order to make comparisons. We then decrease R_N to enhance E_J in order to observe the pair tunnel current. A difference is that we cannot use very large currents with BSCCO due to the current limits for BSCCO damage (to be discussed below). This limitation also impacts the determination of R_N . Since the energy gap of BSCCO is much larger than that of Pb it is more difficult to measure R_N from the *I-V* curves because of the limits on maximum current. Our procedure is to record several *I-V* curves by sweeping the bias voltage above the Pb

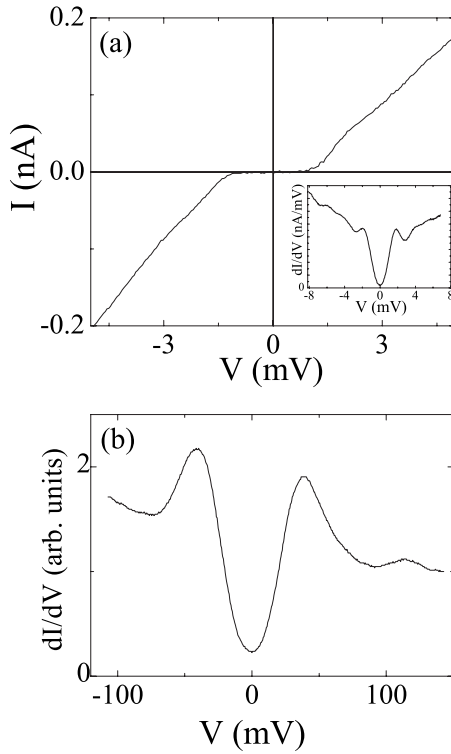


FIG. 9. (a) I - V characteristic of Pb/I/overdoped BSCCO STM junctions at $T=2.1$ K clearly showing a Pb gap around 1.4 meV. Note the absence of leakage although the Pb gap edge is smeared compared to that of Pb/I/Pb STM junctions due to finite states all the way to the Fermi energy in the BSCCO density of states. Inset: dI/dV for the Pb gap taken at $R_N=10$ M Ω . The conductance outside the Pb gap is affected by a relatively large energy gap of BSCCO ($\Delta_{\text{BSCCO}}=40$ meV). (b) dI/dV spectrum taken over a large voltage range for the BSCCO gap at the same location. $R_N=500$ M Ω . The modulation amplitude added to the bias voltage is 2.5 mV_{RMS}.

gap. Then R_N is determined by making use of our knowledge that the junction normal resistance inside the BSCCO gap (above the Pb gap) is 3–4 times larger than that outside the BSCCO gap determined from the dI/dV spectrum such as illustrated in the inset of Fig. 10. For the lower junction resistance I - V curves, R_N was calculated from the factor required to scale the current so that it overlaps with already normalized $I(V)R_N$ versus V curves with the ratio of the conductance inside to that outside the BSCCO gap. A set of dI/dV data for the BSCCO gap and I - V curves taken with progressively lower junction resistances are necessary to calculate the $I_C R_N$ product every time the tip is moved to a new location.

In the main frame of Fig. 10 we plot the I - V characteristics at lower bias and lower R_N . A low leakage current below the Pb gap confirms the high quality of the vacuum tunnel junctions. Further decreasing R_N increases the quasiparticle tunneling probability and finally the contribution from the thermally fluctuated Josephson currents is observed when E_J is comparable to $k_B T_n$.³⁶

Figure 11 displays a close-up view of the I - V characteristics near zero bias clearly showing that the superconducting Pb tip was Josephson coupled to the BSCCO. The quasipar-

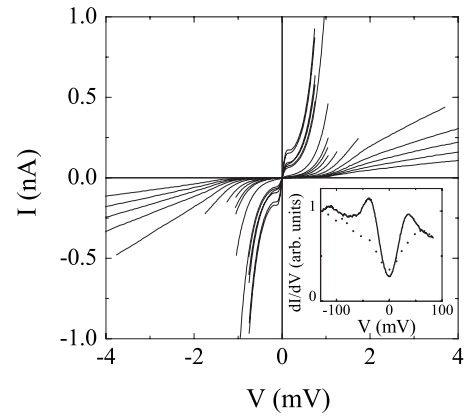


FIG. 10. I - V characteristics of Pb/I/overdoped BSCCO ($T_C=79$ K) STM Josephson junctions at $T=2.1$ K. The Pb gap is clearly seen around $V=1.4$ mV. Inset: dI/dV spectrum (solid line) measured before low R_N measurements showing sharp coherence peaks with $\Delta=37$ meV. dI/dV spectrum measured after low R_N measurements (dotted line) indicates an LDOS change due to high current density.

ticle background represented by the dotted line in Fig. 11(b) is obtained from an average of several normalized I - V curves at higher R_N . At high R_N there is no contribution from the Josephson effect and we use this curve as background. We scale it to the R_N of the lower resistance data and the difference shown in Fig. 11(b) is due to the Josephson currents.

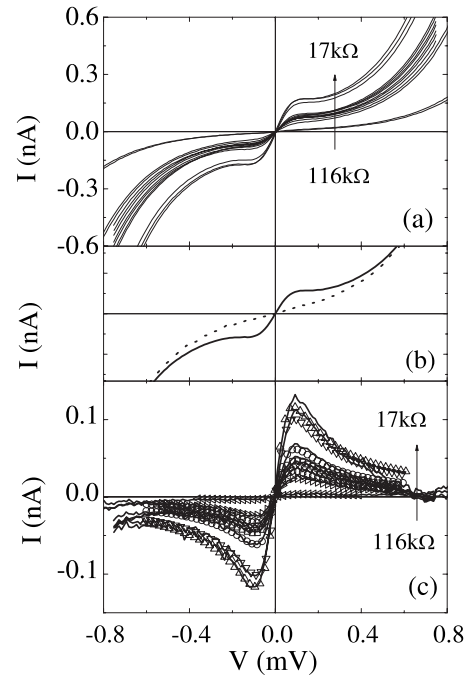


FIG. 11. (a) Low bias I - V characteristics of Fig. 10 for various junction resistances at $T=2.1$ K. (b) Averaged I - V characteristic near zero bias for quasiparticle background (dotted line). One of the observed I - V curves is shown by the solid line. (c) Thermally fluctuated Josephson currents peaked at V_p as derived by subtracting quasiparticle background [Fig. 11(b)] from the I - V curves [Fig. 11(a)]. The data are represented by the lines and the symbols represent two-parameter fits to the phase diffusion model.

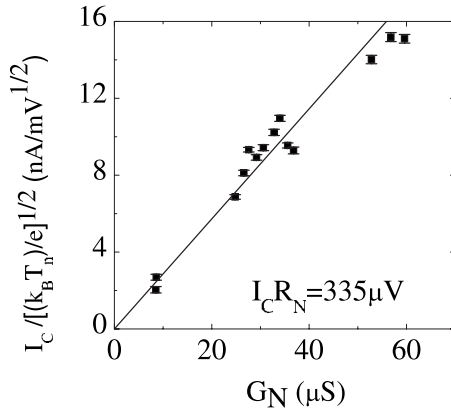


FIG. 12. Plot of $I_C \times \sqrt{e/k_B T_n}$ vs G_N of Pb/I/overdoped BSCCO ($T_C=79$ K) STM Josephson junctions. The slope is equal to $I_C R_N \times \sqrt{e/k_B T_n}$. Using the fitted slope and substituting the previously determined T_n , the Josephson product at this surface point is found to be $I_C R_N = 335 \mu\text{V}$.

Figure 11(c) shows the remaining contributions from the thermally fluctuated Josephson current after subtracting the quasiparticle background of Fig. 11(b) from the I - V curves of Fig. 11(a). The data in Fig. 11(c) are shown as lines and the best fits to the Eq. (2) are represented by the symbols. These good fits convince us that we have likely observed the pair current between a conventional (s -wave) superconducting Pb tip and overdoped BSCCO. This suggests that the BSCCO does not have a pure d -wave order parameter at least at the surface. In addition, the dI/dV spectrum represented by the dotted line in the inset of Fig. 10 was observed after the lowest R_N measurements in Fig. 11. The LDOS has changed significantly during the measurements and the quasiparticle coherence peaks have disappeared perhaps due to the high current density of the measurements at the highest conductance studied. This “modified” dI/dV curve resembles those previously observed in heavily underdoped BSCCO,^{7,9,10} in the “pseudogap” state at temperatures above T_C (Refs. 7 and 37), and in strongly disordered BSCCO thin films.³⁸ It is also similar to the dI/dV spectra observed by others on surfaces which were altered by scanning with large tunnel currents.⁵ It is important to note that LDOS changes were observed only after measurements were made with R_N below 30 k Ω and I above the threshold current around 500 pA. Moreover, the Josephson current disappeared after these irreversible changes in the LDOS on BSCCO occurred. In order to avoid this effect, most of the data presented here were obtained with R_N ranging from 30 to 100 k Ω . This effect will be discussed in subsequent sections.

Each fit to the Josephson portion of the I - V curves in Fig. 11(c) generates a single data point in the plot shown in Fig. 12 in the similar way as described in the Pb/I/Pb and Pb/I/NbSe₂ STM junction results. As G_N is increased (R_N is reduced) the observed I_C increases (E_J increases). We now rely on the values for T_n and Z_{ENV} that we determined from our measurements on Pb/I/Pb for this experimental apparatus, and taking the slope of the linear fit shown in Fig. 12, we find $I_C R_N$ at this surface point to be 335 μV .

There are numerous normal tip STM studies of BSCCO aimed at developing a spatial picture of the electronic quan-

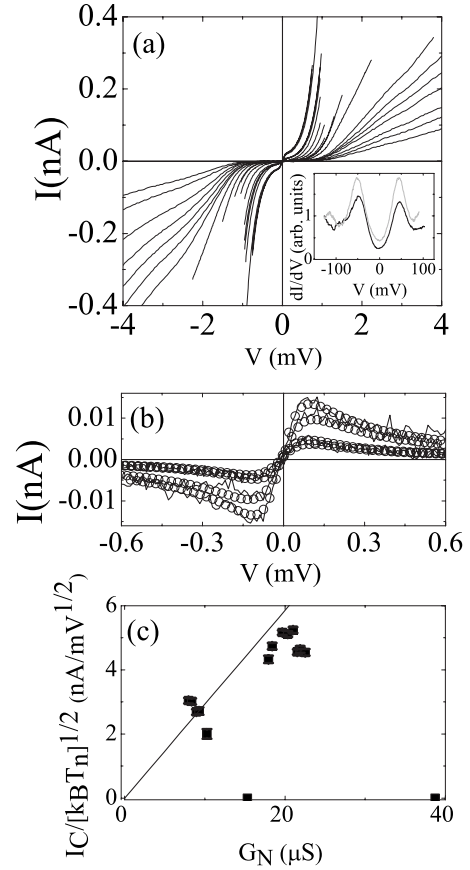


FIG. 13. I - V characteristics of Pb/I/overdoped BSCCO ($T_C=79$ K) STM Josephson junctions at different location from that in Fig. 10. (a) I - V characteristics of Pb/I/overdoped BSCCO ($T_C=79$ K) STM Josephson junctions at $T=2.1$ K. Inset: dI/dV measured before low R_N measurement (black line) and after it (gray line). Note that energy gap is unchanged. (b) Thermally fluctuated Josephson currents (lines) and fits (circles) to the phase diffusion model. (c) Plot of $I_C \times \sqrt{e/k_B T_n}$ vs G_N ; $I_C R_N = 279 \mu\text{V}$. Two data points at $G_N = 15$ and $39 \mu\text{S}$ correspond to I - V characteristics without any pair current observed.

ties of this material. Several of these investigations have produced renderings referred to as gap maps.³⁵ These images reveal the inhomogeneous nature of the energy gap⁶ and periodic electronic modulation both inside the vortex cores³⁹ and above T_C .⁴⁰ Again these data were derived from quasiparticle excitation spectra, not probing the superconducting pair state itself. It is natural to ask (i) whether the superconducting order parameter of BSCCO has spatial variation, and (ii) how the superconducting ground state correlates with the quasiparticle excited states (Δ). Since we have the capability to measure both Δ (Fig. 10) and $I_C R_N$ (Fig. 11) at the same location on the surface, we have used these techniques to address these questions. In order to avoid the irreversible change in the LDOS for higher currents (Fig. 10 inset), the minimum junction resistance was kept above 30 k Ω . The result for a second location on overdoped BSCCO ($T_C=79$ K) is presented in Fig. 13. Unlike the case shown in Fig. 10, the inset of Fig. 13(a) shows no appreciable change in the LDOS after the I - V measurement at the lowest R_N . We found $\Delta=47$ meV at this surface point. $I_C R_N$ derived from

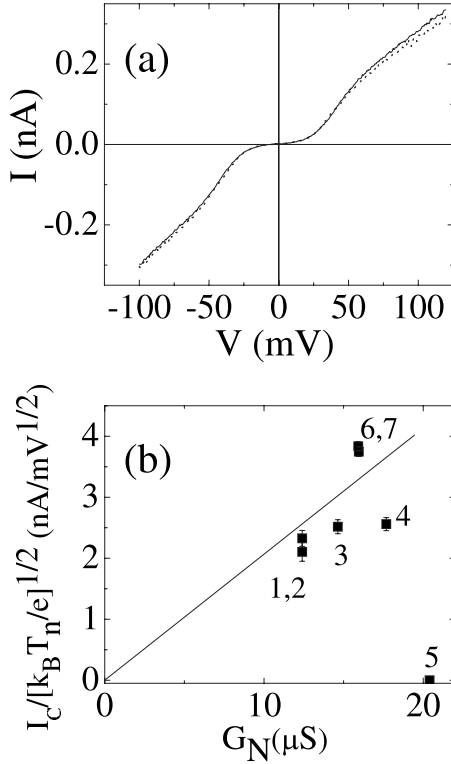


FIG. 14. I - V characteristics and $I_C R_N$ plot of Pb/I/overdoped BSCCO ($T_C=76$ K) STM Josephson junction for studying reproducibility of I_C . (a) I - V curve (solid line) measured before low R_N measurements showing $\Delta=40$ meV. I - V curve measured after low R_N measurements (dotted line) indicating that the energy gap at this surface point remained the same. (b) Plot of $I_C \times \sqrt{e/k_B T_n}$ vs G_N . The number labels represent the chronological order of the data sets. This order clearly shows the Josephson currents disappearing (5) and reappearing (6 and 7). Data points of (1,2) and (6,7) were measured repeatedly at $R_N=80$ and 63 k Ω , respectively.

these data is also different from the previous location.

Of note in Fig. 13(c) are two data points showing zero I_C appearing in the $I_C R_N$ plot. The disappearances of I_C are observed at $G_N=15$ and 39 μS (I - V curves without any Josephson contributions). In order to check reproducibility of the pair current, we first repeated the Josephson current measurement at the same R_N as that when currents had been observed. We also checked the linear relationship between I_C and G_N (both increasing and decreasing G_N). Reproducibility was usually observed. However, occasionally I_C disappeared. Figure 14 shows the $I_C R_N$ plot of Pb/I/overdoped BSCCO ($T_C=76$ K) measured at $T=2.1$ K. We first measured the I - V characteristic for the BSCCO gap [solid line in Fig. 14(a)]. Then R_N was decreased to see the Josephson current on the I - V characteristics. In Fig. 14(b), each Josephson measurement is labeled in the chronological order in which it was taken. The Josephson coupling increases as we decrease R_N (expected) but then unexpectedly disappears at a lower R_N (label 5). Increasing R_N (decreasing G_N) results in the Josephson coupling returning (labels 6 and 7). This behavior is all unexpected. After these low R_N measurements, the large bias I - V curve was again recorded to observe the BSCCO gap. This curve (dashes) in Fig. 14(a) indicates that

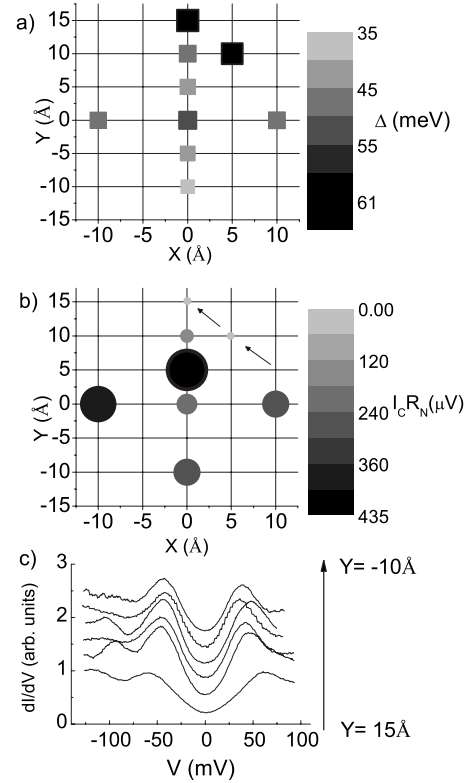


FIG. 15. Spatial studies of both (a) Δ and (b) $I_C R_N$ at the same locations on overdoped BSCCO ($T_C=79$ K). $I_C R_N$ changes spatially and seems to anticorrelate with Δ . Note that no Josephson contributions were observed at the surface points denoted by arrows [in (b)] where the largest energy gaps were measured in this 20 $\text{\AA} \times 25$ \AA region. (c) The line cut of dI/dV spectra is measured along the y axis in (a) showing a well-known gap inhomogeneity (offset for clarity).

the LDOS of the BSCCO and the energy gap remains the same before and after the low R_N measurements so that the disappearance of I_C was not caused by the LDOS change due to high current density. Although the origin of this disappearance is still under investigation, we observe that low R_N measurements (R_N below ~ 300 k Ω) on BSCCO increase the low frequency noise on the tunnel current. This noise appears to be induced locally on the BSCCO and not from the environment or the electronics. These effects were not ever seen in our Josephson studies on the Pb-Pb or NbSe₂ systems. We assure ourselves that we have not affected the tip during the measurements by verifying that the Pb gap is always reproduced and the exponential decrease in the tunnel current vs the tip-sample distance is also observed after low R_N measurements.

Keeping these observations in mind, we performed both local Josephson and spectroscopic measurements on the overdoped BSCCO surface ($T_C=79$ K). Figure 15 shows the spatial dependence of the energy gap and $I_C R_N$ measured simultaneously every 5 – 10 \AA on a particular region on the surface. It clearly indicates that $I_C R_N$ and therefore the superconducting pair wave function of BSCCO changes on a nanometer-length scale on the surface. More interestingly, we can see an anticorrelation between Δ and $I_C R_N$ such that

$I_C R_N$ tends to be reduced as Δ increases. This is not predicted by the BCS theory where Δ_{BCS} and $I_C R_N$ are linearly correlated. The tendency was also observed in the data taken along a line of 100 Å on another overdoped BSCCO ($T_C = 76$ K) sample. This relationship is more apparent when $I_C R_N$ is plotted in the next section as a function of Δ for a variety of experiments.

V. DISCUSSION

A. *d*-wave superconductors

The observation of *c*-axis Josephson coupling in planar Pb-YBa₂Cu₃O_{7- δ} (YBCO) single-crystal Josephson junctions has been reported and was explained by an *s*-wave component in the order parameter of YBCO induced by an orthorhombic distortion.¹⁹ Although the crystallographic symmetry of Bi₂Sr₂CaCu₂O_{8+ δ} (BSCCO) makes *s*- and *d*-wave mixing less likely,⁴¹ Josephson coupling in planar junctions between conventional superconductors and BSCCO has been observed.^{20,21} $I_C R_N$ values for these junctions (Nb- or Pb-BSCCO) ranged from 1 to 10 μV suggesting that the *s* component is about three orders of magnitude smaller than the *d* component. Because $I_C R_N$ was measured in macroscopic junctions in previous work, any strong local inhomogeneities were obscured and meaningful comparisons with an inhomogeneous Δ could not be made. It is, therefore, very important to locally probe the order parameter in this strongly inhomogeneous material using Josephson tunneling.

For high- T_C superconducting cuprates where the pairing mechanism is still under debate, attempts to extract the possible coupling due to the strong electron-phonon interaction were done for YBa₂Cu₃O_{7- δ} although the authors cautioned that the gap observed in the normalized conductance data for YBa₂Cu₃O_{7- δ} is not of the BCS form. Nevertheless, the expected T_C was calculated from the normal state parameters, $\alpha^2 F(\omega)$ and λ derived from the observed dI/dV spectrum and found that it was 2/3 of the measured T_C of this material.⁴²

Recently microscopic studies of the phonon structure by STM were performed for Bi₂Sr₂CaCu₂O_{8+ δ} (Ref. 43) and electron-doped cuprate, Pr_{0.88}LaCe_{0.12}CuO₄.⁴⁴ They have, however, extracted the phonon energies from positive peaks of d^2I/dV^2 spectra, with an assumption that the observed gap was equal to the superconducting gap rather than following the previous procedure. Furthermore, it has been suggested that their results could be interpreted as inelastic tunneling associating with apical oxygen within the barrier.^{45,46} Electrons tunneling from the STM tip can lose energy to an oxygen vibrational phonon mode inside the barrier yielding a new tunneling channel and mimicking the results reported. Furthermore, angle-resolved photoemission spectroscopy (ARPES) data have been interpreted within the context of a strong electron-phonon interaction model.⁴⁷

B. Variation in $I_C R_N$ in overdoped Bi₂Sr₂CaCu₂O_{8+ δ}

We interpret these results within the framework of the phase diagram for high- T_C superconducting cuprates proposed by Emery and Kivelson.⁴⁸ High- T_C superconducting

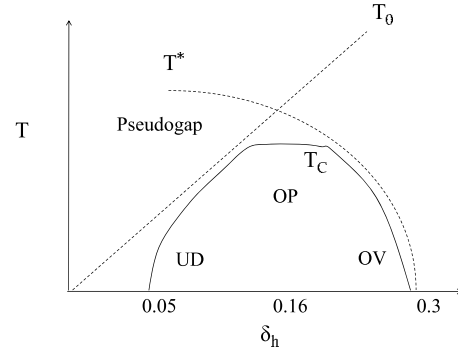


FIG. 16. Phase diagram based on the phase fluctuation model of high- T_C superconductors as functions of temperature T and hole doping, δ_h , proposed by Emery and Kivelson. Optimally doped (OP) region is a crossover from underdoped (UD) to overdoped (OV) region. The phase ordering temperature, T_θ , and the mean-field transition temperature, T^* , are defined in the text.

cuprates are doped Mott insulators with low superfluid density, n_s . Therefore, the phase stiffness, which is the energy scale to twist the phase, is small in these superconductors such that phase fluctuations could play an important role in determining T_C . There are two possible temperature scales that could affect the transition to superconductivity. T_θ is a temperature at which the phase ordering disappears because the phase stiffness disappears. Another temperature scale, T^* , is described as the temperature below which a gap on the quasiparticle spectrum appears. On the low doping side, a system could be divided into regions where the order parameter is well defined *locally* but not globally (a granular superconductor where the grains are weakly coupled to each other). These areas become larger with increasing doping resulting in stronger intergranular coupling so that the phase coherence length becomes longer and less susceptible to phase fluctuations. T_θ is increased as the hole doping δ_h increases leading to a rise of the global T_C of the sample. Meanwhile, T^* continues to decrease as δ_h increases. At the optimal doping, T_θ and T^* cross over, so that the whole sample region is now phase coherent but the mean-field value (energy gap) of the sample is suppressed. Thus, T_θ and T^* are the upper bounds to T_C . T_θ is more significant due to the phase fluctuations on the lower doping side (underdoped), while T^* is more important on the higher doping side (overdoped). Figure 16 plots T_C vs hole doping, δ_h , based on this Emery-Kivelson model and the superconducting region forms a dome shape with the maximum T_C at $\delta_h \sim 0.16$ (optimally doped). Decreasing or increasing δ_h from this value results in a T_C decrease.

In order to interpret our results using this Emery-Kivelson model (T_C vs δ_h), we make two assumptions in order to replace δ_h in their model by the energy gap, Δ , which we actually measure in our experiments.³⁶ First of all, T^* changes monotonically with δ_h and decreases as δ_h increases. Previous STM studies^{9,10} reported the spatially averaged gap value monotonically increased from overdoped (the average $\Delta \leq 40$ meV) to underdoped (the average $\Delta \geq 60$ meV), and dI/dV with $\Delta \geq 65$ meV is often observed in heavily underdoped samples to no longer exhibit sharp coherence peaks. We also measured three samples with different dopings: un-

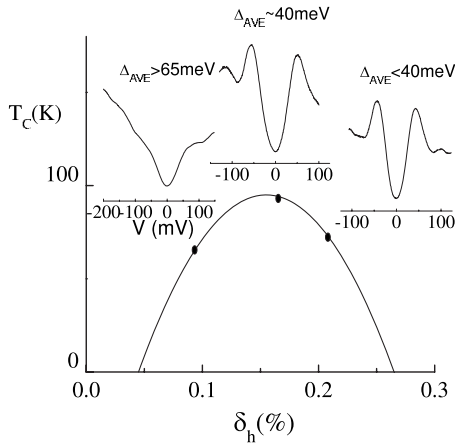


FIG. 17. Typical dI/dV spectra and the corresponding averaged energy gaps, Δ_{AVE} , at $T=2.1$ K for BSCCO with three different dopings. They are underdoped ($T_C=64$ K), optimally doped ($T_C=94$ K), and overdoped ($T_C=76$ K) samples. Note that Δ_{AVE} monotonically decreases as δ_h increases.

derdoped ($T_C=64$ K), optimally doped ($T_C=94$ K), and overdoped ($T_C=76$ K) and observed this tendency as shown schematically in Fig. 17. The results indicate that the average Δ , Δ_{AVE} , seems to monotonically increase as δ_h is decreased. It was reported that the formation of gapped regions obtained from the dI/dV spectra actually started above T_C and there is a linear relation between Δ and the gap opening temperature, T^* , for optimally doped and overdoped BSCCO samples.⁷ Combining with all these facts, we suggest that the δ_h axis in the Emery-Kivelson model can be transformed into the Δ axis, but now T^* monotonically increases with Δ_{AVE} as shown in Fig. 18.

Second, McElroy *et al.*⁹ reported that all the gap-map studies for different dopings, ranging from underdoped to overdoped, show not only strong gap inhomogeneity over all samples, overdoped or underdoped (observation of the larger gap in regions of the overdoped and that of the smaller gap in regions of the underdoped samples), but also the shape of the averaged dI/dV spectra for a given gap seems to be very similar, independent of whether the bulk sample is overdoped or underdoped. These lead us to make the second assumption that although the bulk (macroscopic) doping of each BSCCO sample is characterized by the transport T_C and the spatially averaged energy gap, Δ_{AVE} , local doping which will determine the local superconducting nature of the sample (the locally measured Δ , the pair amplitude, T_C) reflects the observed inhomogeneity. Putting it another way, the smaller gap region which is sparsely distributed on the underdoped sample behaves as “overdoped,” while the larger gap region which is rarely observed in overdoped sample behaves as “underdoped.” This suggestion is also supported by the recent finding of local Fermi surface variations on BSCCO indicating that local doping is not equivalent to the macroscopic doping of the sample.⁴⁹

Since we measure Δ , we choose to replot the Emery-Kivelson model schematically as shown in Fig. 18. We flip the T_C vs δ_h relation in the Emery-Kivelson model to a T_C vs Δ_{AVE} relation. Thus, the region, where the smaller gap is

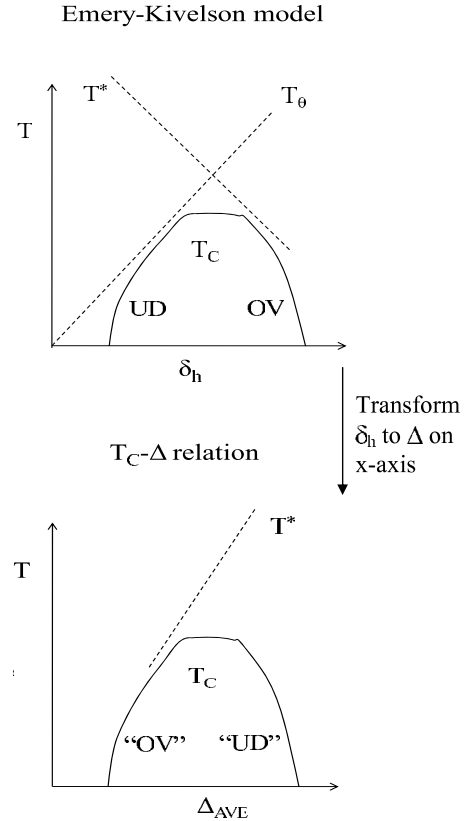


FIG. 18. Modified Emery-Kivelson model which includes two assumptions: (1) the linear relation between Δ and T^* and (2) a local doping variation on the BSCCO surface.

measured, we regard as an overdoped region, while the region with larger gap is regarded as underdoped region, even though our local Josephson measurements are done on overdoped samples ($T_C=76, 79,$ and 81 K). Now T^* (and delta) monotonically increases and the dome-shaped region is simply flipped horizontally as shown when plotted vs Δ .

With this adaptation in hand, we now summarize our measurements of the Josephson $I_C R_N$ product vs Δ for five overdoped samples with each data point taken at locations roughly $5-10$ Å apart.³⁶ Shown in Fig. 19 is the summary plot with the modified Emery-Kivelson model superimposed. Although there is scatter in the observed $I_C R_N$ values for a given Δ , this figure clearly indicates the nanometer scale inhomogeneities in both $I_C R_N$ and Δ . The reason for the scatter from experiment to experiment is under investigation. We believe this scatter is related to the microscopic inhomogeneities of BSCCO. We do not see this kind of scatter in the investigations of Pb/Ag or NbSe₂. A consistent but surprising feature seen from this plot is that $I_C R_N$ tends to be a maximum when Δ is between 40 and 45 meV, and the trend is for it to decrease or become zero as Δ increases or decreases from this maximal point.

Our results in Fig. 19 show that $I_C R_N$ is maximized at a gap value of 40–45 meV, the average Δ typically observed in optimally doped BSCCO (corresponding to the highest T_C samples). $I_C R_N$ decreases as Δ becomes larger. It also decreases as Δ becomes smaller. The $I_C R_N$ vs Δ that we measure behaves in a similar way as T_C vs δ_h (as δ_h changes

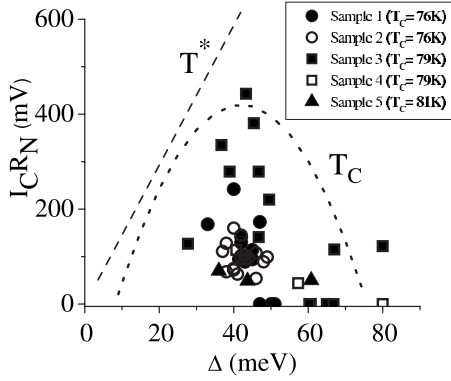


FIG. 19. $I_C R_N$ vs Δ overlaid with the Emery-Kivelson model. Sketches of T_C and T^* from the Emery-Kivelson model are shown by dotted and dashed lines, respectively. The vertical scale for the model curves is arbitrary (obtained from Ref. 36).

toward zero from the critical doping ~ 0.3 at the end of the superconducting region), and it does not follow the behavior of Δ vs T_C as expected from BCS theory. It is important to reiterate that for any given sample, we observed inhomogeneities both in Δ and $I_C R_N$ values as a function of location.

From our results we correlate the observed $I_C R_N$ with the amplitude of the superconducting order parameter $|\Psi|$ as well as with the T_C of BSCCO via the Emery-Kivelson model phase diagram.³⁶ On the underdoped side of the phase diagram, these three quantities ($I_C R_N$, $|\Psi|$, and T_C) decrease (smaller superfluid density) as Δ increases and anticorrelate with T^* . This inverse relation between $I_C R_N$ and Δ in BSCCO is an unconventional result because in the BCS picture Δ_{BCS} , $I_C R_N$, $|\Psi|$, and T_C are all correlated. On the overdoped side of the phase diagram, T_C decreases as δ_h is increased above 0.16 (Δ also becomes smaller in this doping region; a conventional result). Since the overdoped side is the amplitude dominated region, T^* closely relates to Δ and hence decreases as δ_h is increased. $I_C R_N$ decreases as Δ is decreased from the value around 40 meV in Fig. 19 indicating $I_C R_N$, $|\Psi|$, T_C , Δ , and T^* behave similarly and conventionally as δ_h is increased toward the critical doping ($\delta_h \sim 0.3$) where T_C vanishes.

Another possible framework for discussing our results is the two-gap scenario observed in recent ARPES measurements.^{50,51} In the underdoped regime in BSCCO samples, a smaller energy gap is observed and it becomes larger with increasing doping in the nodal region distinct from the larger energy gap (pseudogap) in the antinodal region where no coherence peaks are observed. Moreover, a temperature dependence of the nodal gap follows the BCS functional form very well, while the antinodal gap remains finite at T_C . The same trend of $\Delta(T)$ is also observed in overdoped samples, but the gapless region above T_C expands on the Fermi surface with increasing doping (suppression of the pseudogap). It has also been reported that two gaps are observed in overdoped $(\text{Bi}_{1-y}\text{Pb}_y)_2\text{Sr}_2\text{CuO}_{6+x}$ using a variable temperature STM.⁵² It was claimed that there are smaller homogeneous energy gaps vanishing near T_C as measured from the dI/dV spectra normalized by normal state conductance, as well as the larger inhomogeneous energy

gaps, which have very weak temperature dependence. Although consistent with our $I_C R_N$ measurements, we do not observe the second gap *directly*. To our knowledge, the momentum k component of the tunneling electron parallel to the junction barrier is conserved in the tunnel process, but the very small confinement of the electron due to the STM tip might increase the uncertainty of momentum and relax the constraint for momentum conservation. Thus, the tunneling current observed in the STM could possibly be averaged over a large fraction of the momentum space, therefore, making it difficult to resolve a momentum-dependent gap by STM. Moreover, the results in Fig. 19 represent measurements of both $I_C R_N$ and Δ averaged over momentum space, and therefore we are unable to address this alternate model.

C. Current density effect

We have observed notable changes in the LDOS after low R_N (high current density) measurements. Most of these observations involve preliminary results and more studies are necessary to come to a quantitative conclusion. Nevertheless, we have observed this effect so often that it deserves reporting. The effect is illustrated in the inset of Fig. 10. Several questions arise: Does the LDOS change suddenly or continuously? When or at what R_N does it happen? How does LDOS change relate to the Josephson current? We performed “back and forth” measurements in which the BSCCO gap (high R_N measurement) was measured followed by low R_N measurements at the same location on the surface. Results are shown in Fig. 20. We first measured dI/dV labeled 1, then measured $I-V$ characteristics at lower voltages in the region of the Pb gap. R_N is lowered until it reaches that of the $I-V$ curve labeled 7. The tip is backed up to increase R_N to measure dI/dV for the BSCCO gap labeled 8 and so on. It is interesting that the BSCCO gap remains almost unchanged after measuring the Pb gap at $R_N=68$ k Ω , but a large LDOS change is observed (dI/dV labeled 20) after obtaining the $I-V$ curve labeled 19 at $R_N=11$ k Ω . The dI/dV curve labeled 20 indicates not only a disappearance of sharp coherence peaks but an apparent increase in the energy gap size. Further decreasing R_N to measure the Pb gap ($I-V$ curve labeled 24) makes the LDOS change to a “V” shape (dI/dV labeled 25) where we can no longer define an energy gap. From similar measurements, we have observed that the BSCCO gap and the shape of dI/dV rarely change by measuring the Pb gap until R_N is reduced to around 30 k Ω , but further decreasing R_N causes a deformation of LDOS. Howald *et al.* observed qualitatively similar dI/dV curves on the intentionally disordered surface by scanning with large tunnel current.⁵ Their tunnel condition, however, was at $I=500$ pA with $V=-200$ mV so the power dissipated from the tip was 10^{-10} W, while the typical tunnel condition used in these current measurements for the $I-V$ curve at $R_N=30$ k Ω , for example, is $I=500$ pA with $V=1.2$ mV so that the power dissipated from the superconducting tip is 100 times smaller than that used by Howald *et al.* although tip-sample distance in our STM junctions is smaller. In this configuration the current density, j , could be calculated using the tunnel current $I=500$ pA and the effective diameter of the superconducting

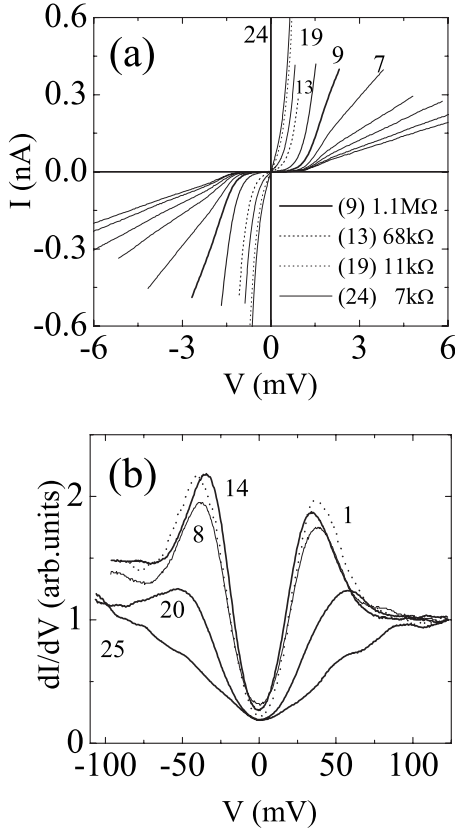


FIG. 20. (a) I - V characteristics and (b) dI/dV spectra taken at the same surface point on overdoped BSCCO ($T_C=74$ K) at $T=2.1$ K. LDOS change in this sample is caused by low R_N measurements. The numbers labeled for I - V and dI/dV curves are measured in chronological order. For example, dI/dV spectrum (14) is taken right after I - V curve (13) was measured.

tip, ~ 3 Å, over which electrons are being injected. Thus, it yields $j \sim 10^6$ A/cm², a very high current density. It is still under investigation to answer why $R_N \sim 30$ kΩ is the threshold resistance for the BSCCO's LDOS change. We conclude that current density is the relevant parameter that causes these surface and spectral changes.

We have also measured the lateral range of the high current density alteration of the LDOS by moving the tip away from the original altered location to measure dI/dV curves a few nanometers away. Figure 21 shows the degraded LDOS is continuously changing, finally recovering to the superconducting LDOS as the tip is moved away from the originally damaged point. The dI/dV spectrum with sharp coherence peaks is recovered at 13 nm away from the damaged point in opposite directions along a line. While Howald *et al.* "burned" the surface by scanning with a large tunnel current, we burned at a specific surface point by taking I - V characteristics at low R_N . It is interesting to note that spatial destruction of the BSCCO superconducting LDOS is similar for both experiments. Only qualitative studies of the high current density effect on BSCCO's electronic structure have been done so far, however, a relation between the thermally fluctuated Josephson current and LDOS change is still unknown. Further study is necessary to discuss this effect quantitatively.

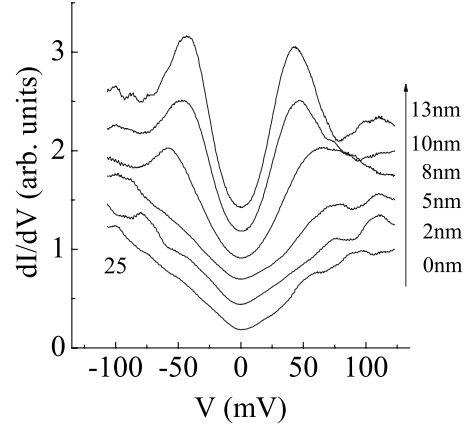


FIG. 21. dI/dV spectra taken along a line from the originally damaged surface point (offset for clarity). The bottom curve is the same dI/dV spectrum labeled 25 in Fig. 20(b).

D. Different surface preparation

Cleaving the BSCCO to expose an atomically flat surface is widely used for STM studies of this material; however, no study of the effect of the cleaving on the electronic structure of BSCCO has been reported. This fact results in a question as to whether the gap inhomogeneity routinely observed on cleaved surfaces is intrinsic to BSCCO or a result of the cleave. It is well known that the superconducting tunneling probes the depth of a coherence length into the sample surface. Therefore it is important to address this question because the electronic degradation on the surface of BSCCO could affect its tunneling current due to the very short c -axis coherence length ($\xi_c \leq 1$ nm) compared with much longer ξ_c of conventional superconductors. Chemical etching is an alternate method to remove a degraded surface layer and possibly make a passivated layer. A chemical etching technique, originally reported by Vasquez *et al.*⁵³ was applied to Pb/I/YBCO tunnel junctions^{54,55} and Josephson junctions.¹⁹ An STM study of etched YBCO single crystals^{56,57} revealed that etching with 1% bromine (Br) by volume in methanol resulted in an etching rate of 250 Å/min. The etching proceeds layer by layer and results in large flat areas separated by steps with single unit cell depth (~ 12 Å). The etching also produced pits on the surface which expand radially, introducing some surface roughness, but further etching removed layers without increasing roughness.

For BSCCO single crystals, we observed that 1% Br in methanol was strong enough to dramatically roughen the etched surface causing the STM to tip crash. This result suggests that BSCCO is more sensitive to the etching than YBCO. In order to optimize the etching condition, etching rate calibrations were performed as follows: the BSCCO single crystal was coated with thinned rubber cement leaving a small region of exposed BSCCO. The etching solution consisting of 0.1% Br in methanol was kept on the BSCCO single crystal for 3 min. The surface was then rinsed by dipping the sample in methanol in an ultrasound cleaner and the rubber cement was removed by sonication in toluene. A commercial profiler revealed clear steps at various edges of the etched region of roughly 6000 Å in height. This result

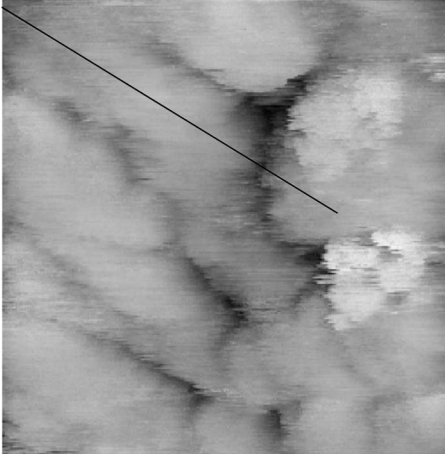


FIG. 22. STM image of 0.1% Br etched overdoped BSCCO ($T_C=74$ K) at room temperature. Scan size is $800 \text{ \AA} \times 800 \text{ \AA}$.

indicates etch rates for BSCCO using 0.1% Br of $2000 \text{ \AA}/\text{min}$.

Figure 22 shows a typical surface of overdoped BSCCO ($T_C=74$ K) etched in 0.1% Br in methanol for 3 min followed by sonication in methanol and finally blown dry with nitrogen gas. The etched surface consists of “pancakes” with lateral dimensions approximately a few hundred angstroms. These pancakes have various step heights of not only a half unit cell in depth, 15 \AA (Fig. 23), but also 5 and 10 \AA . Figure 24 shows a large area scan of the same sample as Fig. 22. A vertical corrugation over this surface is less than 30 \AA indicating that the 0.1% Br etching proceeds layer by layer.

Figure 25 shows the dI/dV spectra measured on the 0.1% Br etched overdoped BSCCO sample at $T=4.2$ K. Two dI/dV curves were taken 10 \AA apart. It is noteworthy that the spectral line shape looks very similar to that observed on the cleaved BSCCO sample except the asymmetry typically observed for cleaved samples in the coherence peaks is reversed. Nevertheless, the result is reproducible. This sample was then cooled to $T=2.1$ K to measure the Pb gap. Figure 26 shows the $I-V$ characteristic measured at a lower R_N . The Pb gap was clearly seen around $V=1.4$ mV although the $I-V$ curve was not taken at the same surface point as Fig. 26. Further investigation is required to determine whether the gap inhomogeneity is intrinsic to this material. It would also be useful to study how the dI/dV spectra and the Josephson $I_C R_N$ product vary over an etched surface.

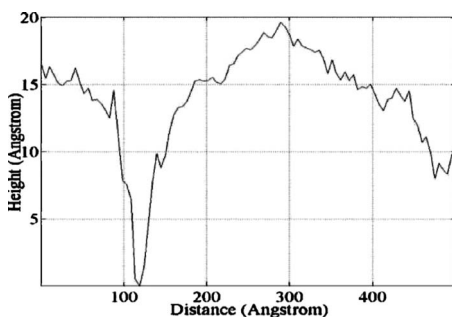


FIG. 23. Surface height cross section along the line shown in Fig. 22.

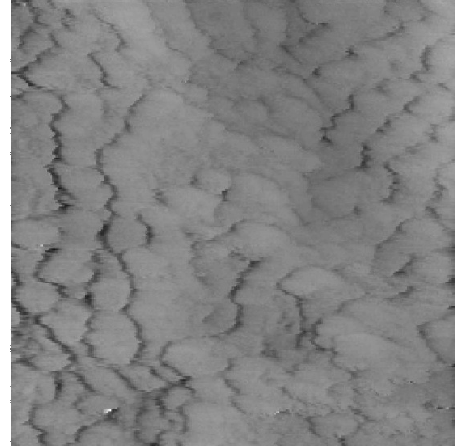


FIG. 24. Room-temperature STM image of the same surface in Fig. 22 with larger scan area ($3200 \text{ \AA} \times 3200 \text{ \AA}$).

It is shown from these preliminary experiments that the Br etching proceeds layer by layer on BSCCO and yields a passivated surface. Observations of the superconducting Pb gap ensure that the passivated layer is thin enough for vacuum tunneling; however, difficulty in reproducible observation of the Pb gap suggests that the thickness might change from etched sample to sample. Low temperature image scans also appear noisier than room-temperature images and there is difficulty at obtaining reproducible low temperature images. Since Br must be handled under a fume hood because of its high volatility and toxic nature, the etching process is done in air. This constraint possibly results in surface contamination although it still remains puzzling why the image is better (less noisy and reproducibly obtained) at room temperature than at low temperature.

In summary, we have prepared the BSCCO surface by chemical etching for our superconducting STM study. The etched BSCCO surface yields reproducible dI/dV spectra; however, extensive low R_N measurements to observe Josephson current have not been accomplished yet.

VI. CONCLUSION

We have described a series of experiments that utilize a superconductor-tipped STM to perform Josephson tunneling

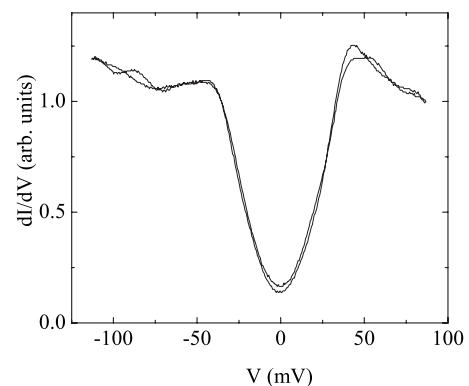


FIG. 25. dI/dV spectra with a large bias measured on the 0.1% bromine etched overdoped BSCCO at $T=4.2$ K. Two dI/dV spectra were measured 10 \AA apart.

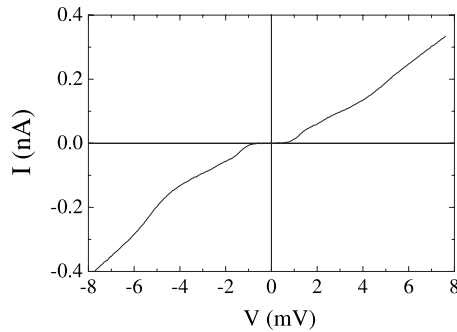


FIG. 26. I - V characteristic measured at lower R_N on the 0.1% bromine etched overdoped BSCCO at $T=2.1$ K. The Pb gap is clearly seen around $V=1.4$ mV.

measurements on the high- T_C superconducting cuprate BSCCO. These measurements are motivated by the desire to directly access the pair wave function given the lack of a theory to connect the quasiparticle DOS to the superconducting state, in contrast to BCS superconductors. Operation of the apparatus has been verified by measurements of a conventional superconductor, Pb, and then the layered superconductor NbSe₂. We find good agreement between these measurements and theoretical predictions giving us confidence in our BSCCO data for which no prediction is available. Our results indicate that like the quasiparticle DOS, the pair wave

function is also inhomogeneous over the doping range studied, with variations on length scales of roughly 1 nm. Furthermore, we find that the gap measured from the quasiparticle DOS is anticorrelated with the Josephson $I_C R_N$ product for areas where the local superconducting nature has the characteristics and is consistent with underdoped samples. In addition we observe that excessive current densities can irreversibly alter the LDOS in these samples and we have determined a limit on the current. Taking care to stay below those limits allows us to avoid this effect. In an effort to determine whether the local inhomogeneities are intrinsic or the result of the surface preparation by cleaving, we have also performed measurements of BSCCO samples that have been etched with a Br/methanol solution. Although no Josephson signal has been detected, this approach does appear to yield reasonable surfaces, albeit with apparent tip contamination challenges.

ACKNOWLEDGMENTS

We thank the Berkeley Physics Machine shop for expert technical assistance and Garg Assoc Pvt Ltd. for providing low noise miniature coax cable. The work in Berkeley was supported by DOE Grant No. DE-FG02-05ER46194. S.O. was supported by KAKENHI Grant No. 20740213 and Y.A. by KAKENHI Grants No. 19674002 and No. 20030004.

*Present address: Department of Physics and Astronomy, University of California, Irvine, California 92697, USA.

†rdynes@ucsd.edu

- ¹I. Maggio-Aprile, C. Renner, A. Erb, E. Walker, and Ø. Fischer, *Phys. Rev. Lett.* **75**, 2754 (1995).
- ²C. Renner, B. Revaz, K. Kadowaki, I. Maggio-Aprile, and Ø. Fischer, *Phys. Rev. Lett.* **80**, 3606 (1998).
- ³S. H. Pan, E. W. Hudson, A. K. Gupta, K.-W. Ng, H. Eisaki, S. Uchida, and J. C. Davis, *Phys. Rev. Lett.* **85**, 1536 (2000).
- ⁴S. H. Pan, J. P. O'Neal, R. L. Badzey, C. Chamon, H. Ding, J. R. Engelbrecht, Z. Wang, H. Eisaki, S. Uchida, A. K. Gupta, K.-W. Ng, E. W. Hudson, K. M. Lang, and J. C. Davis, *Nature (London)* **413**, 282 (2001).
- ⁵C. Howald, P. Fournier, and A. Kapitulnik, *Phys. Rev. B* **64**, 100504(R) (2001).
- ⁶K. M. Lang, V. Madhavan, J. E. Hoffman, E. W. Hudson, H. Eisaki, S. Uchida, and J. C. Davis, *Nature (London)* **415**, 412 (2002).
- ⁷K. K. Gomes, A. N. Pasupathy, A. Pushp, S. Ono, Y. Ando, and A. Yazdani, *Nature (London)* **447**, 569 (2007).
- ⁸A. N. Pasupathy, A. Pushp, K. K. Gomes, C. V. Parker, J. Wen, Z. Xu, G. Gu, S. Ono, Y. Ando, and A. Yazdani, *Science* **320**, 196 (2008).
- ⁹K. McElroy, D.-H. Lee, J. E. Hoffman, K. M. Lang, J. Lee, E. W. Hudson, H. Eisaki, S. Uchida, and J. C. Davis, *Phys. Rev. Lett.* **94**, 197005 (2005).
- ¹⁰J. W. Alldredge, J. Lee, K. McElroy, M. Wang, K. Fujita, Y. Kohsaka, C. Taylor, H. Eisaki, S. Uchida, P. J. Hirschfeld, and J. C. Davis, *Nat. Phys.* **4**, 319 (2008).

- ¹¹V. Ambegaokar and A. Baratoff, *Phys. Rev. Lett.* **10**, 486 (1963).
- ¹²O. Naaman, W. Teizer, and R. C. Dynes, *Phys. Rev. Lett.* **87**, 097004 (2001).
- ¹³O. Naaman, R. C. Dynes, and E. Bucher, *Int. J. Mod. Phys. B* **17**, 3569 (2003).
- ¹⁴O. Naaman, W. Teizer, and R. C. Dynes, *Rev. Sci. Instrum.* **72**, 1688 (2001).
- ¹⁵A. S. Katz, A. G. Sun, R. C. Dynes, and K. Char, *Appl. Phys. Lett.* **66**, 105 (1995).
- ¹⁶M. Hansen, *Constitution of Binary Alloys*, 2nd ed. (McGraw-Hill, New York, 1958).
- ¹⁷H. F. Hess, R. B. Robinson, and J. V. Waszczak, *Physica B* **169**, 422 (1991).
- ¹⁸T. Yokoya, T. Kiss, A. Chainani, S. Shin, M. Nohara, and H. Takagi, *Science* **294**, 2518 (2001).
- ¹⁹A. G. Sun, D. A. Gajewski, M. B. Maple, and R. C. Dynes, *Phys. Rev. Lett.* **72**, 2267 (1994).
- ²⁰M. Mößle and R. Kleiner, *Phys. Rev. B* **59**, 4486 (1999).
- ²¹I. Kawayama, M. Kanai, M. Maruyama, A. Fujimaki, and H. Hayakawa, *Physica C* **325**, 49 (1999).
- ²²S. Ono and Y. Ando, *Phys. Rev. B* **67**, 104512 (2003).
- ²³S. H. Pan, E. W. Hudson, and J. C. Davis, *Appl. Phys. Lett.* **73**, 2992 (1998).
- ²⁴Y. M. Ivanchenko and L. A. Zil'berman, *Zh. Eksp. Teor. Fiz.* **55**, 2395 (1968) [*Sov. Phys. JETP* **28**, 1272 (1969)].
- ²⁵G.-L. Ingold, H. Grabert, and U. Eberhardt, *Phys. Rev. B* **50**, 395 (1994).
- ²⁶Y. Harada, H. Takayanagi, and A. A. Odintsov, *Phys. Rev. B* **54**, 6608 (1996).

- ²⁷R. Ono, M. Cromar, R. Kautz, R. Soulen, J. Colwell, and W. Fogle, *IEEE Trans. Magn.* **23**, 1670 (1987).
- ²⁸J. Martinis and R. Kautz, *Phys. Rev. Lett.* **63**, 1507 (1989).
- ²⁹R. Kautz and J. Martinis, *Phys. Rev. B* **42**, 9903 (1990).
- ³⁰G.-L. Ingold and Yu. V. Nazarov, in *Single Charge Tunneling*, edited by H. Grabert and M. Devoret (Plenum, New York, 1992).
- ³¹O. Naaman, Ph.D. thesis, University of California–San Diego, 2003.
- ³²T. A. Fulton and D. E. McCumber, *Phys. Rev.* **175**, 585 (1968).
- ³³O. Naaman and R. C. Dynes, *Solid State Commun.* **129**, 299 (2004).
- ³⁴P. W. Anderson, in *Lectures on the Many-Body Problem, Ravello 1963*, edited by E. R. Caianello (Academic Press, New York, 1964), Vol. II, pp. 113–135.
- ³⁵Ø. Fischer, M. Kugler, I. Maggio-Aprile, C. Berthod, and C. Renner, *Rev. Mod. Phys.* **79**, 353 (2007).
- ³⁶H. Kimura, R. P. Barber, Jr., S. Ono, Y. Ando, and R. C. Dynes, *Phys. Rev. Lett.* **101**, 037002 (2008).
- ³⁷C. Renner, B. Revaz, J.-Y. Genoud, K. Kadowaki, and Ø. Fischer, *Phys. Rev. Lett.* **80**, 149 (1998).
- ³⁸T. Cren, D. Roditchev, W. Sacks, J. Klein, J.-B. Moussy, C. Deville-Cavellin, and M. Laguës, *Phys. Rev. Lett.* **84**, 147 (2000).
- ³⁹J. E. Hoffman, E. W. Hudson, K. M. Lang, V. Madhavan, H. Eisaki, S. Uchida, and J. C. Davis, *Science* **295**, 466 (2002).
- ⁴⁰M. Vershinin, S. Misra, S. Ono, Y. Abe, Y. Ando, and A. Yazdani, *Science* **303**, 1995 (2004).
- ⁴¹J. F. Annett, N. Goldenfeld, and S. R. Renn, in *Physical Properties of High Temperature Superconductors II*, edited by D. M. Ginsberg (World Scientific, Teaneck, NJ, 1990).
- ⁴²R. C. Dynes, F. Sharifi, and J. M. Valles, Jr., in *Proceedings of the Conference on Lattice Effects in High- T_C Superconductors*, edited by Y. Bar-Yam, T. Egami, J. Mustre-Leon, and A. R. Bishop (World Scientific, Singapore, 1992), pp. 299–308.
- ⁴³J. Lee, K. Fujita, K. McElroy, J. A. Slezak, M. Wang, Y. Aiura, H. Bando, M. Ishikado, T. Masui, J.-X. Zhu, A. V. Balatsky, H. Eisaki, S. Uchida, and J. C. Davis, *Nature (London)* **442**, 546 (2006).
- ⁴⁴F. C. Niestemski, S. Kunwar, S. Zhou, S. Li, H. Ding, Z. Wang, P. Dai, and V. Madhavan, *Nature (London)* **450**, 1058 (2007).
- ⁴⁵S. Pilgram, T. M. Rice, and M. Sigrist, *Phys. Rev. Lett.* **97**, 117003 (2006).
- ⁴⁶D. J. Scalapino, *Nat. Phys.* **2**, 593 (2006).
- ⁴⁷A. Lanzara, P. V. Bogdanov, X. J. Zhou, S. A. Kellar, D. L. Feng, E. D. Lu, T. Yoshida, H. Eisaki, A. Fujimori, K. Kishio, J.-I. Shimoyama, T. Noda, S. Uchida, Z. Hussain, and Z.-X. Shen, *Nature (London)* **412**, 510 (2001).
- ⁴⁸V. J. Emery and S. A. Kivelson, *Nature (London)* **374**, 434 (1995).
- ⁴⁹W. D. Wise, M. C. Boyer, K. Chatterjee, T. Kondo, T. Takeuchi, H. Ikuta, Y. Wang, and E. W. Hudson, *Nat. Phys.* **5**, 213 (2009).
- ⁵⁰K. Tanaka, W. S. Lee, D. H. Lu, A. Fujimori, T. Fujii, Risdiana, I. Terasaki, D. J. Scalapino, T. P. Devereaux, Z. Hussain, and Z.-X. Shen, *Science* **314**, 1910 (2006).
- ⁵¹W. S. Lee, I. M. Vishik, K. Tanaka, D. H. Lu, T. Sasagawa, N. Nagaosa, T. P. Devereaux, Z. Hussain, and Z.-X. Shen, *Nature (London)* **450**, 81 (2007).
- ⁵²M. C. Boyer, W. D. Wise, K. Chatterjee, M. Yi, T. Kondo, T. Takeuchi, H. Ikuta, and E. W. Hudson, *Nat. Phys.* **3**, 802 (2007).
- ⁵³R. P. Vasquez, B. D. Hunt, and M. C. Foote, *Appl. Phys. Lett.* **53**, 2692 (1988).
- ⁵⁴M. Gurvitch, J. M. Valles, Jr., A. M. Cucolo, R. C. Dynes, J. P. Garno, L. F. Schneemeyer, and J. V. Waszczak, *Phys. Rev. Lett.* **63**, 1008 (1989).
- ⁵⁵J. M. Valles, Jr., R. C. Dynes, A. M. Cucolo, M. Gurvitch, L. F. Schneemeyer, J. P. Garno, and J. V. Waszczak, *Phys. Rev. B* **44**, 11986 (1991).
- ⁵⁶A. G. Sun, A. Truscott, A. S. Katz, and R. C. Dynes, *Phys. Rev. B* **54**, 6734 (1996).
- ⁵⁷A. Truscott, Ph.D. thesis, University of California–San Diego, 1999.